IEEE Access
Multidisciplinary ⋮ Rapid Review ⋮ Open Access Journal

Received 17 September 2022, accepted 12 October 2022, date of publication 19 October 2022, date of current version 22 December 2022.

Digital Object Identifier 10.1109/ACCESS.2022.3215708

RESEARCH ARTICLE

A Pneumatic Proportional Constant Flow Valve With Mechanical Feedback

SIHAO FU[1], SHUO LIU[1,2,3], YONG CAI[4], JIAJIE MA[4], ZIJING YU[1], WENHAN GAO[1], AND XIAO ZHANG[1]

[1]Ocean Academy, Zhejiang University, Zhoushan 316021, China
[2]Key Laboratory of Ocean Observation-Imaging Testbed of Zhejiang Province, Zhoushan 316021, China
[3]Robotics Institute, Zhejiang University, Yuyao 315400, China
[4]Ocean Research Center of Zhoushan, Zhejiang University, Zhoushan 316021, China

Corresponding author: Shuo Liu (shuoliu@zju.edu.cn)

This work was supported in part by the Pioneer and Leading Goose Research and Development Program of Zhejiang under Grant 2022C03041, in part by the Key Research and Development Project of Zhejiang Province under Grant 2022C04016, and in part by the Institute of Robotics at Zhejiang University under Grant K12002.

ABSTRACT To make the flow rate of a gas valve insensitive to changes in inlet pressure and to achieve proportional constant flow characteristics, a proportional constant flow valve is proposed, which is mechanically fed back by the pressure of the flowing gas itself. Using air as the source, the motion equation of the spool is established according to pneumatic theory. By means of the steady state equation, it is proved that the valve is insensitive to the change of inlet pressure compared with an ordinary proportional valve, and the optimization direction of the valve is analyzed. Based on Amesim software, the entire model of the pneumatic proportional constant flow valve is established, and the flow characteristic parameters of feedback holes with different diameters are obtained by numerical calculation. Subsequently, through overall simulation, we obtain the specific values of the optimization parameters. Finally, relevant experimental tests are conducted. The results show that the optimized proportional constant flow valve with mechanical feedback has a good proportional constant flow effect compared with the ordinary proportional flow valve.

INDEX TERMS Mechanical feedback, air valve, proportional constant flow, numerical calculation.

I. INTRODUCTION

As the name suggests, gas proportional valves are the types of valves specifically used for gas flow or pressure proportional regulation. Gas flow proportional valve is widely used in medical equipment, chemical equipment and so on because of its proportional flow characteristics. Pneumatic proportional technology and hydraulic proportional technology have many similarities, but, because of high compressibility, the flow of gas tends to be more complex, and it can be divided into different flow states according to the pressure ratio between the inlet and outlet of an orifice. The flow rate of gas is not only related to the throttling area, but also influenced by inlet and outlet pressures. Therefore, proportional valves usually require constant inlet pressure to maintain a constant set flow rate. Figure 1 shows the pressure-flow rate curve of an ordinary proportional valve. For occasions where the inlet pressure fluctuates significantly, although there is a small nonlinear segment in the pressure-flow curve, the percentage of flow rate change also has a similar magnitude to the percentage of pressure change. This is fatal for occasions that require high constant flow characteristics such as the proportional adjustment of chemical reaction gasses and medical oxygen concentration [1], [2].

To achieve the goal of the output flow being insensitive to the inlet pressure, in addition to an additional pressure or flow rate feedback adjustment device, the direct use of a constant flow valve can simplify the pneumatic system [3], [4]. Constant flow valves, also known as passive flow control valves, auto regulated valves, or pressure-compensated valves, output a constant flow rate regardless of pressure changes. As it does not require additional energy to drive and has a simple

The associate editor coordinating the review of this manuscript and approving it for publication was Agustin Leobardo Herrera-May.

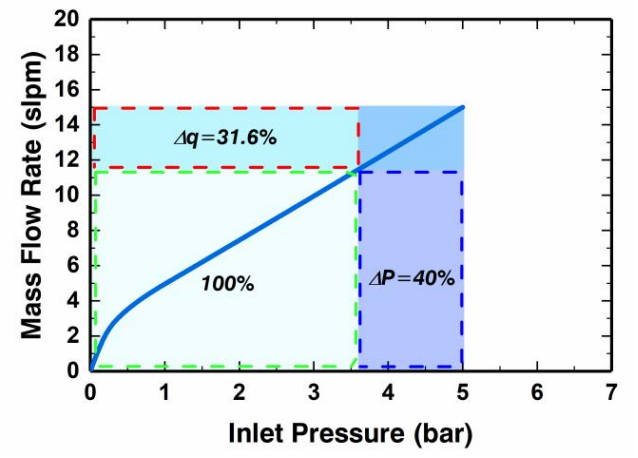

FIGURE 1. Effect of inlet pressure on the output flow rate of an ordinary proportional valve.

and compact structure, constant flow valve is widely used in industrial water treatment, centrifugal pump protection, irrigation, and other fields [5].

At present, there are many research achievements in the field of medical flow regulators. To treat hydrocephalus, for example Eric Chappel of the Leeds University in the United Kingdom developed a flow control valve [6]. The length of the flow channel is related to the pressure gradient of the liquid. When the pressure gradient increases, the length of the channel increases, causing the liquid flow coefficient to decrease. In 1988, Park first used MEMS technology to study a constant flow microregulator based on a flexible membrane; since then, other research groups had conducted more in-depth studies. For example, Dumont-Fillon developed a flow regulator specifically for implantable pumps. The pressure at the inlet and outlet of the flow regulator acts on both sides of the SOI membrane. The SOI membrane has a certain stiffness. When a change in the pressure difference between the two sides occurs, the SOI membrane moves, causing the liquid flow cross-sectional area to change accordingly. Therefore, the output flow is constant [7], [8], [9]. Zhang et al. studied a self-adaptive flexible valve based on a similar application background. He used the deformation of a cantilever-like flap under a change in flow velocity to adjust the flow area of the fluid to realize constant flow rate. In this structure, the choice of material and size of the flap is key as it affects the degree of deformation of the flap in response to flow velocity [10]. In addition to the medical fields, constant flow valves are often used to improve the oil film stiffness of sliding bearings. When the journal is offset, compared to the ordinary restrictor, the restrictor with constant flow valve can maintain the flow rate through the oil chamber constant, so that the bearing with a constant flow valve has greater recovery stiffness, thus improving the working stability and reducing wear [11], [12]. All of these studies are based on passive and output flow rate deterministic working scenarios. Once the corresponding constant flow device is manufactured, the output flow rate is fixed, and it is difficult to adjust the structure according to the need. For situations where proportional control is required, companies such as PONAR Wadowice integrated proportional throttle valve and pressure compensation valves to form proportional flow control valve. When throttle valve has a certain opening degree, the pressure compensation valve can be passively adjusted to cope with the pressure gradient change. While this type of valve solves the requirement for proportional adjustment, it is essentially a combination of throttle valve and compensation valve. Throttle valve spool and compensation valve spool still need to be manufactured separately, and their structure is more complicated than that of a conventional constant flow valve [13]. A pressure compensation method without additional compensation valve or electronic compensation system was investigated using flow force by E. Lisowski et al. and applied it to a multi-stage proportional directional control valve. According to the momentum equation, the axial flow force on a spool is closely related to the jet angle, so they achieved this by setting a suitable spool shape. For sliding valves, the steady-state flow force generally points in the direction that closes the spool. when the flow rate decreases due to pressure changes, the flow force will also decrease, so that the spool opening changes to compensate for the decrease in flow rate, and vice versa [14]. Currently, most of the relevant work in the field of constant flow valves is based on liquid media, and relatively little research has been done on gases, especially supersonic flow gases. In this study, a pneumatic proportional constant flow valve with a simple structure is studied based on the throttling effect of a hole. Firstly, the force of the spool is analyzed, the expression of feedback force is derived, and the steady state equation of the spool is obtained. Secondly, according to the steady-state equation, the constant flow capability of the valve is analyzed and the optimization direction of the valve is determined. Then, the theoretical conclusions are verified by the FEM and related simulation software, and the optimization parameters are determined. Finally, the actual performance of proportional constant current valve is tested by relevant experiments.

II. STRUCTURE AND WORKING PRINCIPLE

The structure of the mechanical feedback pneumatic proportional constant flow valve is illustrated in Figure 2. The valve as a whole is divided into two parts, where I is a proportional electromagnet and II is a proportional constant flow valve. The spool is connected to a feedback membrane using a connector. The feedback membrane is clamped between the valve body and the upper cover. A feedback hole is present at the outlet of the valve body. The valve body, feedback membrane, and sealed cap are enclosed to form a cavity. The exterior of the feedback membrane is exposed to air. The spring is used to provide a preload that keeps the spool pressed against the valve seat.

The working principle of the proportional constant flow valve is shown in Figure 3(a)-(c). When the electromagnet is fed with a certain current, it will generate electromagnetic

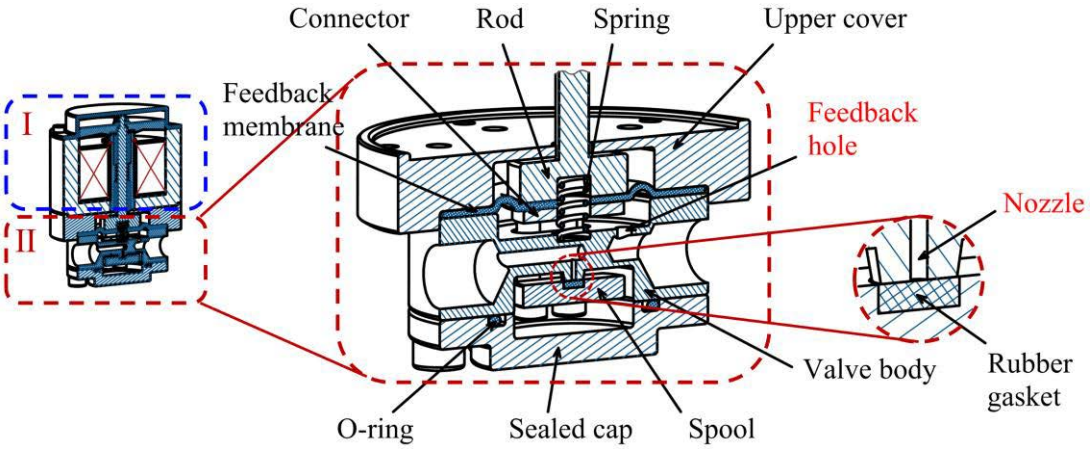

FIGURE 2. Structure of the pneumatic proportional constant flow valve with mechanical feedback. I is the proportional electromagnet and II is the valve part.

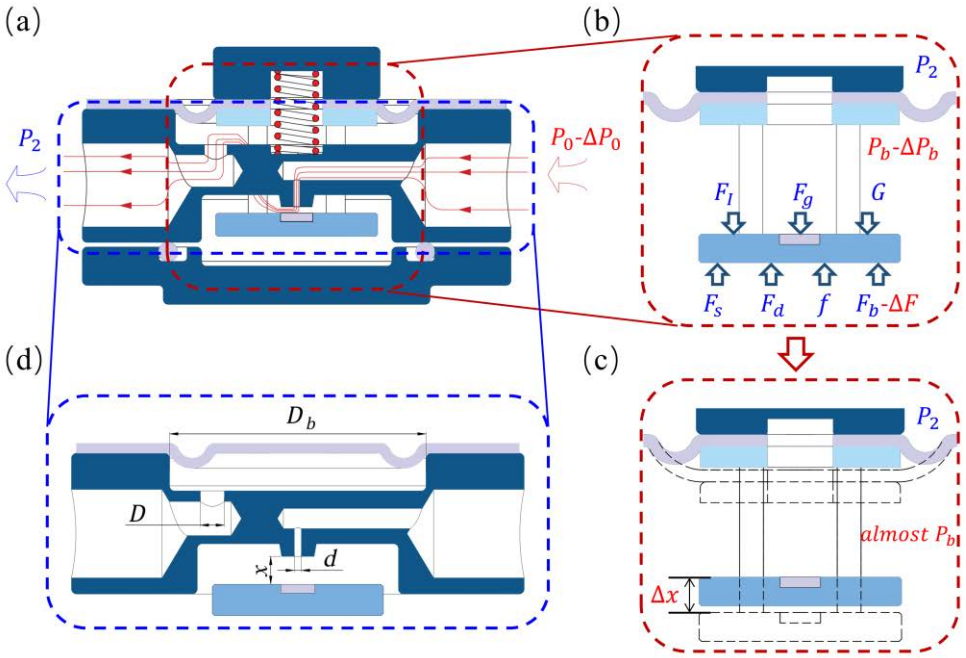

FIGURE 3. (a)–(c) are the working principle of the proportional constant flow valve. (d) shows the key dimensional parameters of the valve.

force F_I to push the spool open. Under the inlet pressure P_0 and outlet pressure P_2, gas flow occurs. By adjusting the current of the electromagnet, the proportional adjustment of flow rate can be achieved. When the inlet pressure decreases, the flow rate decreases. Owning to the throttling effect of the feedback hole, the cavity pressure decreases, too. Relying on the transmission of the feedback membrane and connector, the feedback force F_b acting on the spool is reduced. Therefore, the spool is unbalanced and moves in the direction of increasing the opening degree to compensate for the reduced flow rate. The same principle is applied when the inlet pressure increases. So as to keep flow rate constant.

The design requirements of the pneumatic proportional constant flow valve in this study are listed in Table 1.

A. PNEUMATIC ANALYSIS

As can be seen from Figures 3(a) and 3(b), most of the surface of the spool is affected by the pressure $P_b$in the cavity. Therefore, the feedback force should be the resultant force of P_b acting on the spool and the feedback membrane. The surface of the spool facing the nozzle is subjected to inlet pressure P_0, which results in a force F_g. In addition, other parts that move with the spool are subjected to friction f and air damping F_d, as well as their respective gravity. When the

TABLE 1. Design requirements.

Quantity	Valve	Unit
Electromagnetic driving force	0-15 (Limited by power)	N
Flow rate	0-15	slpm
Air source pressure	3-5 (rated 5)	bar
Outlet pressure	0	bar

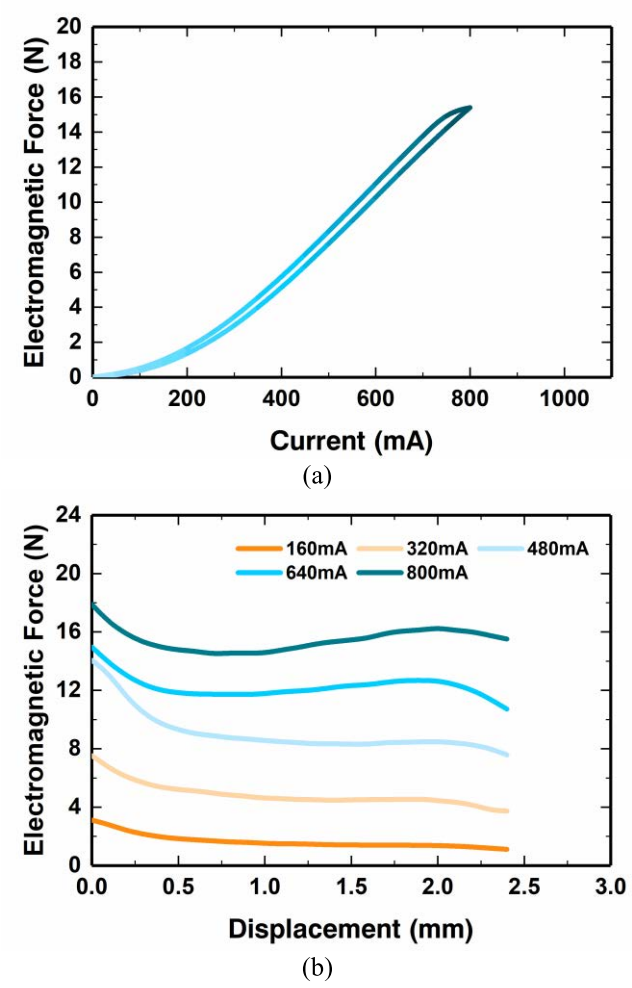

FIGURE 4. (a) Current-force hysteresis curve. (b) Displacement-force curve.

valve is not working, the spool is also affected by spring force, which keeps the spool tight against the valve seat. Finally, the spool is driven and opened using the electromagnetic driving force F_I generated by an electromagnet. The characteristic curve of the electromagnet is shown in Figure 4 (obtained from experiments). Therefore, according to the force analysis diagram in Fig.3(b), the motion equation of the spool can be written as (1), in which the mass m is the sum of all the moving parts.

$$m\ddot{x} + F_d + F_b + Kx = F_\Sigma - f \tag{1}$$

$$F_\Sigma = F_I + F_g + G - F_{s0} \tag{2}$$

F_Σ is the net driving force without friction, G is the sum of the gravity of all moving parts, and F_{s0} is the preload provided by the spring. All forces except the feedback force F_b can be related to the state quantities (displacement x or velocity $\dot{x}$). For example, the damping force is equal to the velocity multiplied by the damping coefficient, and the friction can be associated with displacement and velocity by sign function (according to the Coulomb model). In order to obtain the expression of the feedback force, a pneumatic analysis is necessary. In this study, we take air as an example and assume that the air inside the valve is an adiabatic isentropic flow. Under the action of the upstream absolute pressure P_u, absolute temperature T_u and downstream absolute pressure P_l, the mass flow rate through an orifice can be calculated by (3) and (4).

$$q_m^* = SP_u\sqrt{\frac{2\kappa}{R\left(\kappa+1\right)T_u}}\left(\frac{2}{1+\kappa}\right)^{\frac{1}{\kappa-1}} \quad in\ \frac{P_l}{P_u} \le b \tag{3}$$

$$q_m = q_m^*\sqrt{1-\left(\frac{\frac{P_l}{P_u}-b}{1-b}\right)^2} \quad in\ 1 \ge \frac{P_l}{P_u} > b \tag{4}$$

$$b = \left(\frac{2}{\kappa+1}\right)^{\frac{\kappa}{\kappa-1}} \tag{5}$$

Due to structural and manufacturing limitations, the diameter of the feedback membrane cannot be very small, so the diameter D_b of the effective part is fixed at 25.5 mm. Considering the limitation of electromagnetic driving force, the pressure difference between the two sides of the feedback membrane and the pressure difference between the two ends of the feedback hole is less than 0.277 bar. Therefore, the air-flow at the nozzle is supersonic, and the feedback hole is subsonic. The subsonic mass flow rate equation is simplified to (6).

In practice, when gas passes through pneumatic components, the value of b is generally between 0.2 and 0.5. Moreover, the pressure difference between the two ends of the feedback hole does not exceed 0.277 bar. Thus, by approximating (6) to (7), the maximum error is only approximately 5 %. Therefore, (7) can be used to calculate the mass flow rate at the feedback hole. Combining (7) with the mass flow rate formula at the nozzle, we can obtain the feedback

pressure expression (8).

$$q_m = q_m^* \sqrt{1 - \left(\frac{\frac{P_l}{P_u} - b}{1-b}\right)^2} = \frac{q_m^*}{P_u}\sqrt{\left[\left(1 - \frac{1}{2-2b}\right)\frac{P_u - P_l}{P_l} + 1\right]\frac{2P_l\left(P_u - P_l\right)}{1-b}} \tag{6}$$

$$q_m = \frac{q_m^*}{P_u}\sqrt{\frac{2P_l\left(P_u - P_l\right)}{1-b}} \tag{7}$$

$$P_{bA} = P_{2A} + \frac{8\left(1-b\right)P_{0A}^2 T_{bA}}{\pi^2 D^4 P_{2A} T_{0A}} S^2 \tag{8}$$

P_{0A}, P_{2A} are absolute pressures for inlet and outlet, respectively. T_{bA} is the absolute temperature of the cavity and can be obtained according to the state equation of the isentropic process, as shown in (9). At the same time, the upstream air state quantities have the relationship shown in (10), so the cavity temperature can be expressed in (11). By simultaneously using (8) and (11), we can derive the cavity pressure expression (12).

$$P_A^{\frac{1}{\kappa}}/\rho = constant \tag{9}$$

$$P_{0A} = \rho_0 R T_{0A} \tag{10}$$

$$T_{bA} = P_{bA}^{\frac{\kappa-1}{\kappa}} P_{0A}^{\frac{1-\kappa}{\kappa}} T_{0A} \tag{11}$$

$$P_{bA} = \frac{8\left(1-b\right)P_{0A}^{\frac{1+\kappa}{\kappa}}}{\pi^2 D^4 P_{2A}} S^2 P_{bA}^{\frac{\kappa-1}{\kappa}} + P_{2A} \tag{12}$$

Since the pressure difference between the valve cavity and the environment is much smaller than the atmospheric pressure and we have $(\kappa - 1)/\kappa = 2/7$ for air. So, the cavity pressure can be approximately written as (13) with a margin of error of no more than 7 %.

$$P_{bA} = \frac{8\left(1-b\right)S^2}{\pi^2 D^4 P_{2A}^{\frac{1}{\kappa}}} P_{0A}^{\frac{1+\kappa}{\kappa}} + P_{2A} \tag{13}$$

Thus, the feedback force F_b is equal to the pressure difference $P_{bA} - P_{2A}$ multiplied by the sum of the effective area of the feedback membrane and cross-sectional area of the nozzle. As in (14)

$$F_b = \left(P_{bA} - P_{2A}\right)\left(\frac{\pi D_b^2}{4} + \frac{\pi d^2}{4}\right) = \frac{2\left(1-b\right)\left(D_b^2 + d^2\right)S^2}{\pi D^4 P_{2A}^{\frac{1}{\kappa}}} P_{0A}^{\frac{1+\kappa}{\kappa}} \tag{14}$$

Because a throttle in the form of a flat valve is used in this study, the effective cross-sectional area S is approximately (15).

$$S = x\pi d \tag{15}$$

Substituting (15) into the feedback force expression (14), and denoting the coefficient by ψ, the feedback force can be written in the form of (16). Since then, all forces in the motion equation can be expressed as functions of state quantities.

$$F_b = \psi x^2 \tag{16}$$

$$\psi = \frac{2\pi\left(1-b\right)\left(D_b^2 + d^2\right)d^2}{P_{2A}^{\frac{1}{\kappa}} D^4} P_{0A}^{\frac{1+\kappa}{\kappa}} \tag{17}$$

$$m\ddot{x} + \zeta\dot{x} + \psi x^2 + K = F_\Sigma - g(x, \dot{x}) \tag{18}$$

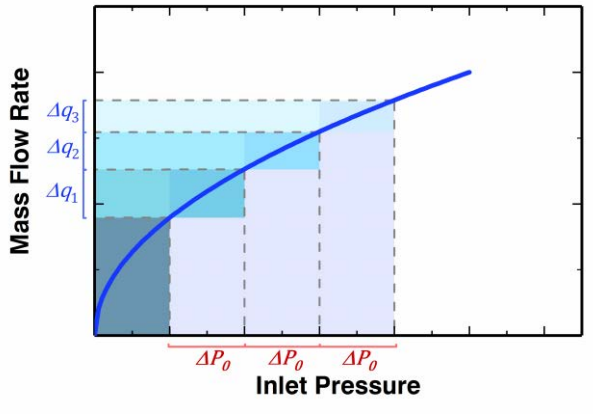

FIGURE 5. Schematic diagram of the effect of changes in inlet pressure on the output flow rate.

B. CONSTANT FLOW CAPACITY ANALYSIS

The purpose of setting the feedback hole is to passively adjust the valve spool opening through feedback force F_b to offset or partially offset the influence of the change in the inlet pressure to achieve a constant flow rate. Therefore, further analysis is required to determine the factors affecting constant flow capability and to prepare for subsequent optimization.

As shown in Figure 5, under a given electromagnet force, when the inlet pressure changes by ΔP_{0A}, the output flow rate will also change by Δq. A smaller value of Δq indicates the change in inlet pressure has less effect on the output flow rate. Therefore, the constant flow capability of the valve within a certain pressure neighborhood can be described as the derivative of the mass flow rate to the pressure, as shown in (19).

$$\frac{dq}{dP_{0A}} = \lim_{\Delta P_{0A} \to 0} \frac{\Delta q}{\Delta P_{0A}} \tag{19}$$

Furthermore, according to the mass flow rate formula for supersonic flow, if the temperature of the air source is almost constant, the mass flow rate is proportional to the product of the inlet pressure and opening degree. Let $\gamma = d(xP_{0A})/(dP_{0A})$, the analysis of the constant flow capability is equivalent to the analysis of γ. Considering the frictionless case, the opening degree at the equilibrium point of the spool can be obtained from the steady state equation of the spool, and the expression for γ is derived (22).

$$x_0 = \frac{2F_\Sigma}{\sqrt{K^2 + 4\psi F_\Sigma} + K} \tag{20}$$

$$x_0 P_{0A} = \frac{2P_{0A}F_\Sigma}{\sqrt{K^2+4\psi F_\Sigma}+K} \tag{21}$$

$$\begin{aligned}\gamma &= \frac{d\left(x_0 P_{0A}\right)}{dP_{0A}} \\ &= \frac{\frac{\kappa-1}{\kappa}F_\Sigma}{\left(\sqrt{K^2+4\psi F_\Sigma}+K\right)} \\ &\quad + \frac{F_g}{\sqrt{K^2+4\psi F_\Sigma}} \\ &\quad + \frac{\frac{1+\kappa}{\kappa}KF_\Sigma}{\left(\sqrt{K^2+4\psi F_\Sigma}+K\right)\sqrt{K^2+4\psi F_\Sigma}}\end{aligned} \tag{22}$$

For an ordinary proportional valve, $x_0 P_{0A}$ has a derivative of (23).

$$\gamma^* = \frac{d\left(x_0^* P_{0A}\right)}{dP_{0A}} = \frac{F_\Sigma^* + F_g}{K^*} \tag{23}$$

K^* is the spring stiffness of the ordinary proportional valve. We select K^* as shown in (24), where ψ_r, $F_{\Sigma rmax}$ are the feedback force coefficient and maximum net driving force respectively under rated pressure. Therefore, the proportional constant flow valve and the ordinary proportional valve have the same maximum net driving force $F_{\Sigma rmax}$ and the same corresponding maximum mass flow rate under rated pressure.

$$K^* = \frac{\left(\sqrt{K^2+4\psi_r F_{\Sigma rmax}}+K\right)}{2} \tag{24}$$

If the spring stiffness K of the proportional constant flow valve is about 0, then the ratio of γ to γ^* is (25) under the same net driving force, where F_Σ varies from 0 to $F_{\Sigma max}$ and P_{0Ar} is rated pressure.

$$\begin{aligned}\delta &= \frac{\gamma}{\gamma^*} \\ &= \frac{\kappa-1}{2\kappa}\left[1+\frac{1}{(\kappa-1)\left(\frac{F_\Sigma}{F_g}+1\right)}\right]\sqrt{\frac{F_{\Sigma max}}{F_\Sigma}\left(\frac{P_{0Ar}}{P_{0A}}\right)^{\frac{1+\kappa}{\kappa}}}\end{aligned} \tag{25}$$

It can be seen that the ratio δ decreases with an increase in the net driving force F_Σ, and increases with an increase in F_g. When F_g is much smaller than F_Σ, δ can be approximated as (26), and when F_g is much larger than F_Σ, δ can be approximated as (27). This shows that only when $F_\Sigma/F_{\Sigma max}$ satisfies (28) will the proportional constant flow valve lose the constant flow capability.

$$\delta \approx \frac{1}{7}\sqrt{\frac{F_{\Sigma max}}{F_\Sigma}\left(\frac{P_{0Ar}}{P_{0A}}\right)^{\frac{1+\kappa}{\kappa}}} \tag{26}$$

$$\delta \approx \frac{1}{2}\sqrt{\frac{F_{\Sigma max}}{F_\Sigma}\left(\frac{P_{0Ar}}{P_{0A}}\right)^{\frac{1+\kappa}{\kappa}}} \tag{27}$$

$$\frac{F_\Sigma}{F_{\Sigma max}} \le \left(\frac{1}{49}\text{to}\frac{1}{4}\right)\left(\frac{P_{0A}}{P_{0Ar}}\right)^{\frac{1+\kappa}{\kappa}} \tag{28}$$

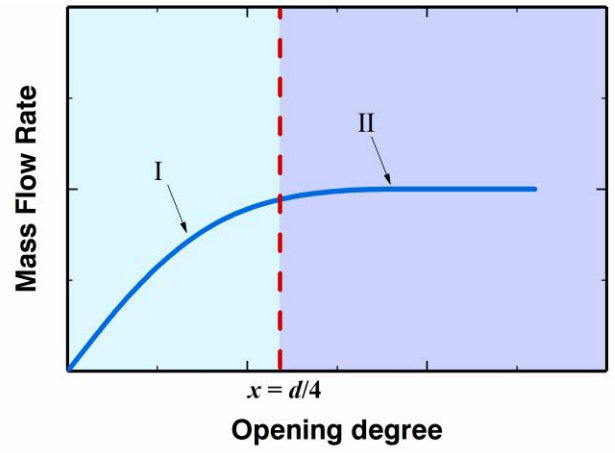

FIGURE 6. Schematic diagram of mass flow rate change with opening degree.

Let $x_0 P_{0A} = Q$, Q is a parameter that characterizes the mass flow rate and there is a relationship as in (29). When the entry temperature is constant, α is constant. Then, from (21), (30) can be obtained

$$q_m = \alpha Q \tag{29}$$

$$F_\Sigma = \frac{\left(P_{0A}QK + \psi Q^2\right)}{P_{0A}^2} \tag{30}$$

Substituting (30) into (22), after simplification, the expression γ with the mass flow rate parameter Q as the independent variable is obtained.

$$\gamma = \frac{(\kappa-1)\,Q}{2\kappa P_{0A}} + \frac{2\,(1+\kappa)\,KQ + \kappa\pi d^2 P_{0A}^2}{4\kappa\,(KP_{0A}+2\psi Q)} \tag{31}$$

Because the larger the net driving force F_Σ is, the smaller the γ is, the optimization problem of the valve can be formulated as follows: under the constraint that the maximum electromagnetic driving force F_{Imax} is not exceeded, the change rate γ is minimized. As shown in (32) and (33).

$$min\ \gamma \tag{32}$$

$$subject\ to\ \ x_{0r}P_{0Ar}|_{F_\Sigma = F_{\Sigma rmax}} = Q_{rmax} \tag{33}$$

x_{0r} — equilibrium position under rated pressure
Q_{rmax} — represents the maximum mass flow rate under rated pressure.

(31) and (33) are combined to eliminate ψ. (34) and (35) can be obtained as follows:

$$\gamma = \frac{(\kappa-1)\,Q}{2\kappa P_{0A}} + \frac{\nu}{4\kappa\xi} + \frac{\mu - \frac{\nu\lambda}{\xi}}{4\kappa\,(\xi K+\lambda)} \tag{34}$$

$$\gamma = \frac{(\kappa-1)\,Q}{2\kappa P_{0A}} + \frac{\nu K+\mu}{4\kappa\,(\xi K+\lambda)} \tag{35}$$

$$\xi = P_{0Ar}^{\frac{1}{\kappa}}Q_{rmax}^2 P_{0A} - 2Q_{rmax}P_{0A}^{\frac{1-\kappa}{\kappa}}Q \tag{36}$$

$$\mu = \pi d^2 P_{0Ar}^{\frac{1}{\kappa}}Q_{rmax}^2 P_{0A}^2 \tag{37}$$

$$\lambda = 2F_{\Sigma rmax}P_{0Ar}P_{0A}^{\frac{1-\kappa}{\kappa}}Q \tag{38}$$

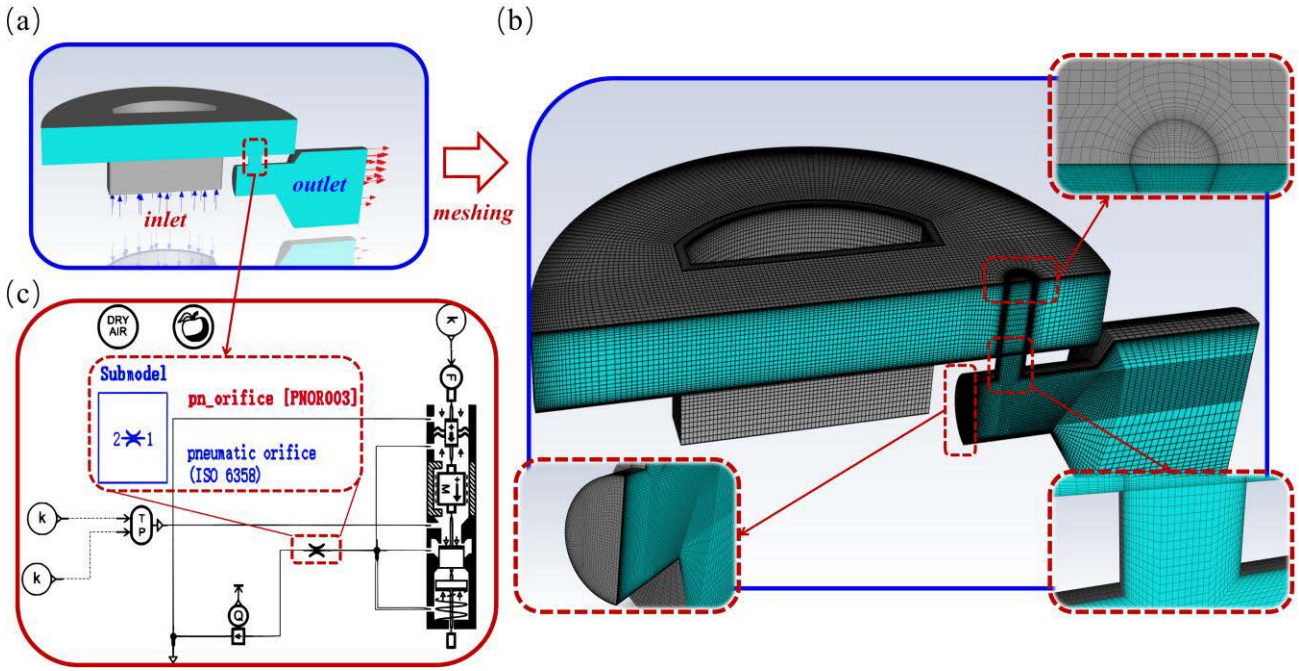

FIGURE 7. (a) Numerical simulation model. (b) Grid division situation. O-grid is used for feedback hole and outlet runner. The whole is divided by structural grid and refined near the walls. The thickness of the first grid layer at the feedback hole near the wall is 0.04 mm. (c) Overall model of the proportional constant flow valve built in AMEsim.

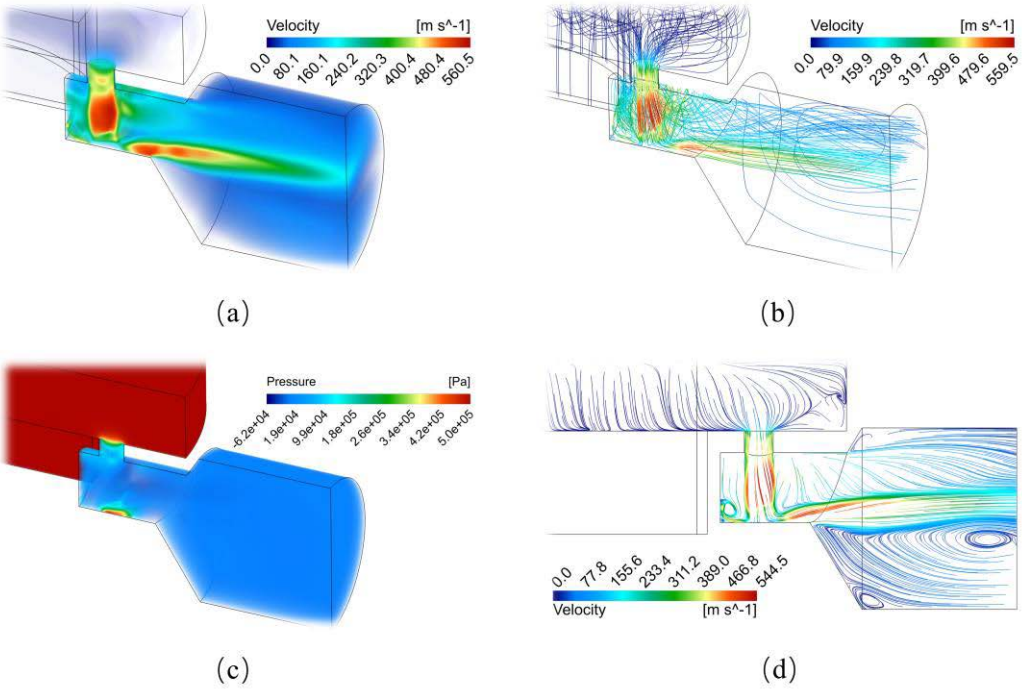

FIGURE 8. (a) Volume rendering for velocity. (b) Overall streamline diagram. (c) The volume rendering of static pressure. (d) The streamline diagram in the symmetric plane.

$$\nu = 2\,(1+\kappa)\,P_{0Ar}^{\frac{1}{\kappa}} Q_{rmax}^{2} Q \tag{39}$$

(34) and (35) show that at each given pressure and mass flow rate point (P_{0A}, Q), the magnitude of γ is related only to the spring stiffness K and nozzle diameter d. It can be concluded that when $\mu > \nu\lambda/\xi$, or the parameter Q is less than a certain value, γ decreases with an increase in the spring stiffness K; when Q is greater than a certain value, γ increases with an increase in K. This shows that for the decrease in γ, increasing the spring stiffness has a positive effect at a low flow rate, but the opposite is true at a large flow rate. In addition, the larger the nozzle diameter d, the larger γ.

TABLE 2. Optimized parameter.

Parameter	Impact
K	At low flow rate, γ decreases with increasing K. At high flow rate, γ increases with K increasing.
d	γ increases as d increases.

TABLE 3. Valve parameters.

Parameter	Valve	Unit
D_b	25.5	mm
m	0.1	kg
P_0	3~5（Rated 5）	bar
P_2	0	bar
F_I	0~15	N
F_{s0}	2	N

In summary, the optimization parameters of the valve are listed in Table 2.

Of course, the value of the nozzle diameter d is limited, because we require the valve to have a constant flow capability within the range of 3-5 bar, and the constant flow capability is achieved by adjusting the valve spool opening degree essentially. Therefore, the adjustable range of the opening degree-flow rate curve should be sufficient, that is, part I of Figure 6.

III. SIMULATION AND OPTIMIZATION

The above discussion mainly introduced qualitative analysis of the mechanical feedback proportional constant flow valve. To optimize the constant flow capacity and obtain the critical size parameters, a quantitative analysis is still required. This study will complete this process with the help of the Fluent and Amesim simulation software.

In the process of theoretical derivation, it is assumed that the flow is isentropic, but due to viscosity and other factors, the actual gas is almost irreversible. There are also van der Waals forces among molecules, so the relationship among the state quantities of gas is often not as simple as the ideal gas law. Therefore, in the simulation, we consider the viscosity of air and use the RK real gas model [15]. In addition, by combining (30) and (33), we find that D, D_b and K are interrelated. For the convenience of numerical simulation and testing, $D_b = 25.5$ mm is fixed, and the optimization of the feedback hole diameter D is used to replace the optimization of the stiffness K. First, we obtain the pneumatic parameters of different feedback hole diameters through Fluent numerical simulation and then use the valve model established by Amesim to conduct the overall simulation. The valve model is shown in Figure 7(c). According to the standard ISO6358, the flow characteristics of an orifice can be described by the critical pressure ratio $b$and sonic conductance C, so we can use the PNOR003 model based on the ISO6358 standard to represent the feedback hole in the simulation model [16]. Other valve parameters are listed in Table 3.

Figure 7(a) shows the numerical simulation model. Because the flow field had a symmetrical structure, the symmetrical simulation method is adopted. Fluent provides a variety of RANS methods, the most commonly used of which are the standard $K-\varepsilon$, standard $K-\omega$ and SST models. $K-\varepsilon$ provides good calculation results for free shear flow, but it is not ideal for the boundary layer flow. Compared with $K-\varepsilon$, $K-\omega$ is better at handling near-wall, adverse pressure

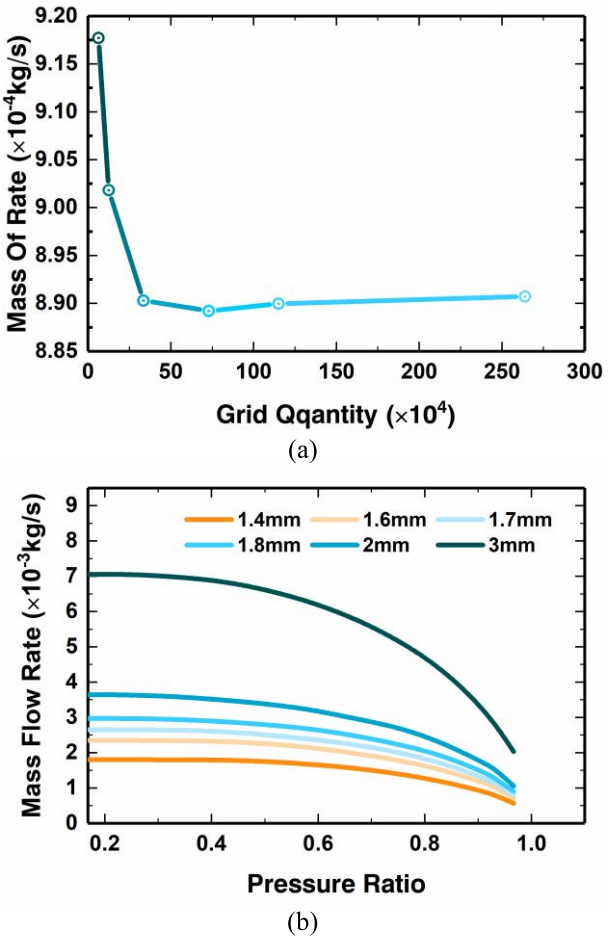

FIGURE 9. Simulation results for different grid numbers (focusing on mass flow rate). (b) Flow characteristic curves for different di-ameters of the feedback hole.

gradient and separation flow problems; however, its ω equation is more sensitive to the main flow field and is not as good as $K-\varepsilon$ for free shear flow. The SST model combines the advantages of $K-\omega$ model and $K-\varepsilon$ model. Therefore, it is more appropriate to use the SST model for the calculations in this study [17], [18]. In order to eliminated the influence of grid number on the results, grid-independence verification was carried out first. The inlet pressure and feedback hole diameter were set to 5 bar and 1.4 mm, respectively. The effect of grid number on the simulation result is shown in Figure 9(a). It can be observed that starting from the grid number about 300,000, the result is stable. Considering the

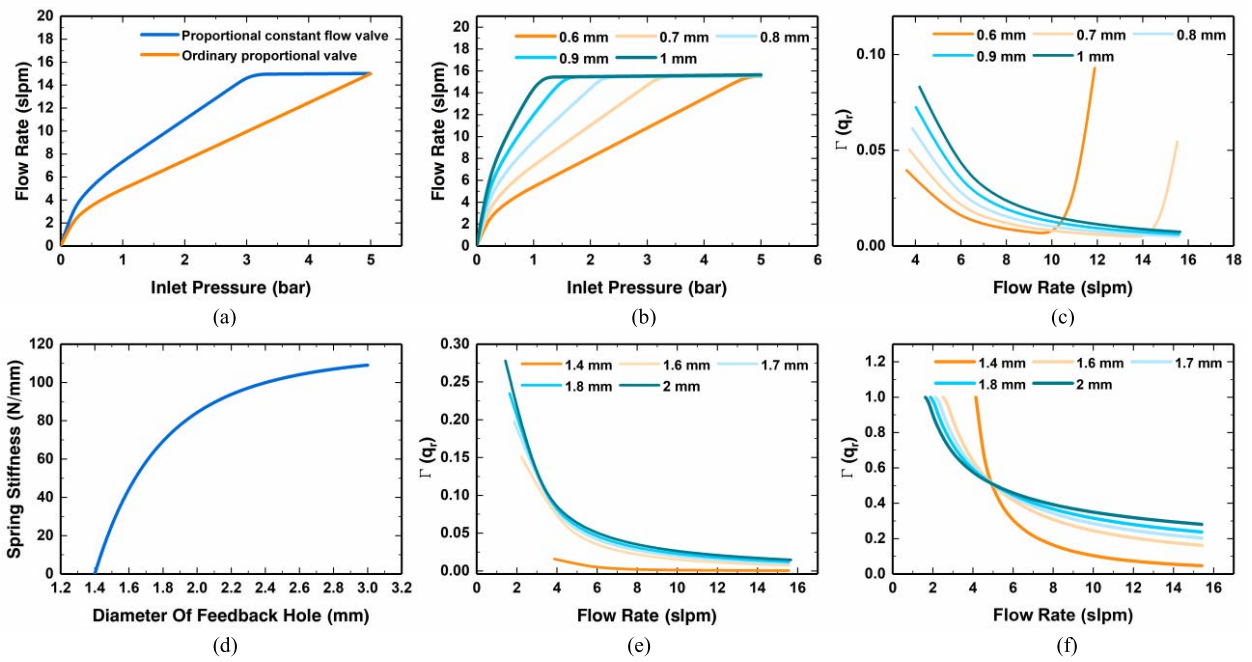

FIGURE 10. (a) Comparison of constant flow performance between ordinary proportional valve and proportional constant current valve. (b) $P_0 - q$ curves for different nozzle diameters. The simulated mass flow rate is half of the total. (c) $q_r - \Gamma(q_r)$ curves for different nozzle diameters. (d) Spring stiffness versus feedback hole diameter for a given driving force of 15 N. (e) $q_r - \Gamma(q_r)$ curves for different feedback hole diameters for a nozzle diameter of 0.8 mm. (f) $q_r - \Gamma(q_r)$ curves for different feedback hole diameters (2.6 mm nozzle diameter).

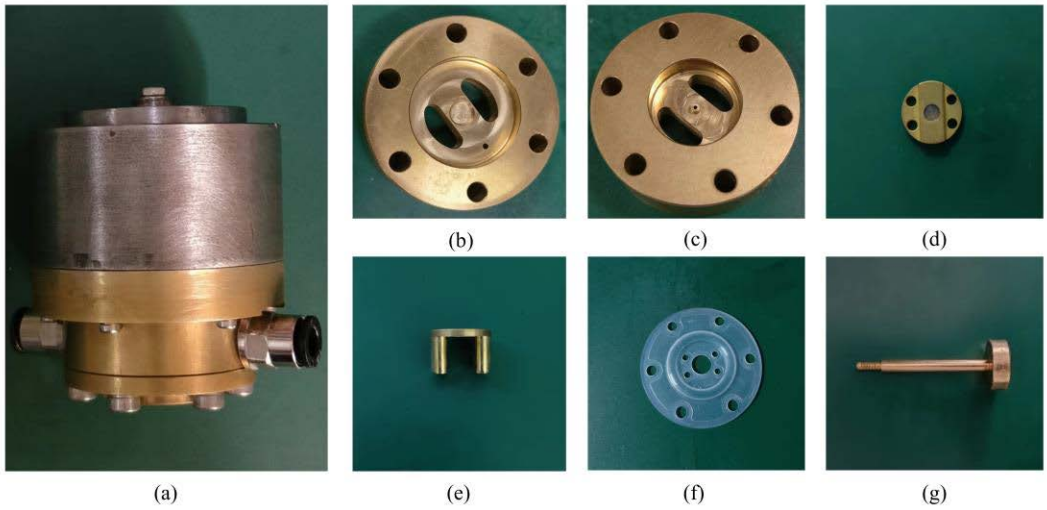

FIGURE 11. (a) Physical map of the proportional constant flow valve. (b) Feedback hole of 1.4 mm diameter. (c) 0.8 mm diameter nozzle. (d) Spool. (e) Connector. (f) Feedback membrane. (g) Rod.

calculation efficiency, a division scheme with grid number of approximately 700,000 is selected. The situation of grid division is illustrated in Figure 7(b). The associated volume rendering and streamline diagram are shown in Figure 8. Because of the small pressure ratio between inlet and outlet, the air flow velocity reaches supersonic at the downstream of feedback hole, and a jet is formed at the outlet.

The flow characteristic curves of the different feedback holes are obtained by simulation, as shown in Figure 9(b). The least-squares method is used to calculate the critical pressure ratio b. According to ISO6358, there is a theoretical formula for the flow conductance ratio, as in (40), where y_i is the ratio of the inlet and outlet pressures of the feedback hole. The simulated flow conductance ratio can be replaced by the mass flow rate ratio as shown in (41). q_m^* is the maximum mass flow rate for each feedback hole diameter. The idea of the least-squares method is to take a difference between the simulated and theoretical conductance ratios at each pressure

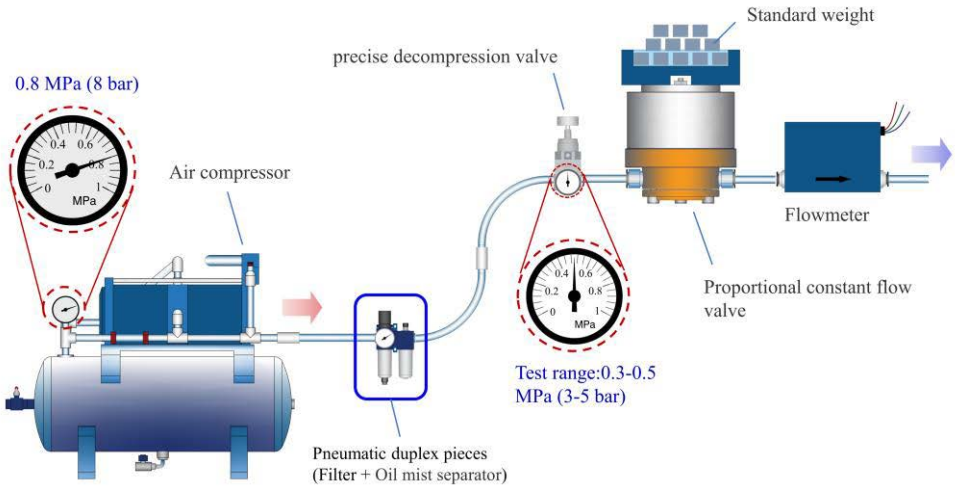

(a)

(b)

FIGURE 12. (a) Schematic diagram of the valve test setup. The filter and oil mist separator are used to eliminate the effect of airborne impurities and oil mist on the measurement results of the thermal flowmeter. (b) Test system physical diagram.

ratio and get the quadratic sum of these differences (42). Then, the critical pressure ratio b is obtained by minimizing the quadratic sum σ.

$$\frac{C_e}{C} = \sqrt{1 - \left(\frac{y_i - b}{1 - b}\right)} \tag{40}$$

$$c = \frac{q_m}{q_m^*} \tag{41}$$

$$\sigma = \sum_{i=1}^{N} \left(c - \sqrt{1 - \left(\frac{y_i - b}{1 - b}\right)} \right)^2 \tag{42}$$

Finally, the values of the flow characteristics parameters for each feedback hole diameter are obtained, as listed in Table 4.

In the AMEsim model, flow characteristic parameters of feedback hole are introduced for the whole simulation. Figure 10(a) shows the inlet pressure-flow rate curve of the proportional constant flow valve and an ordinary proportional valve with a given 15 N driving force, feedback hole diameter of 1.4 mm, and nozzle diameter of 0.7 mm (volume flow rate at normal temperature and pressure). It can be observed that the mechanical feedback valve has a good constant flow-characteristic in a certain inlet pressure range. Figure 10(b) shows the inlet pressure-flow rate curves of different nozzle diameters with a 15 N driving force and 1.4 mm diameter feedback hole. Because we only focus on the flow rate change in the pressure range of 3-5 bar, the constant flow capacity of the valve can be described by

TABLE 4. Flow characteristic parameters.

Diameter of feedback hole D (mm)	critical pressure ratio b	Sonic conductance C(m³/s/Pa)
3	0.215	9.576×10-9
2	0.231	4.947×10-9
1.8	0.277	4.029×10-9
1.7	0.285	3.591×10-9
1.6	0.299	3.185×10-9
1.4	0.329	2.441×10-9

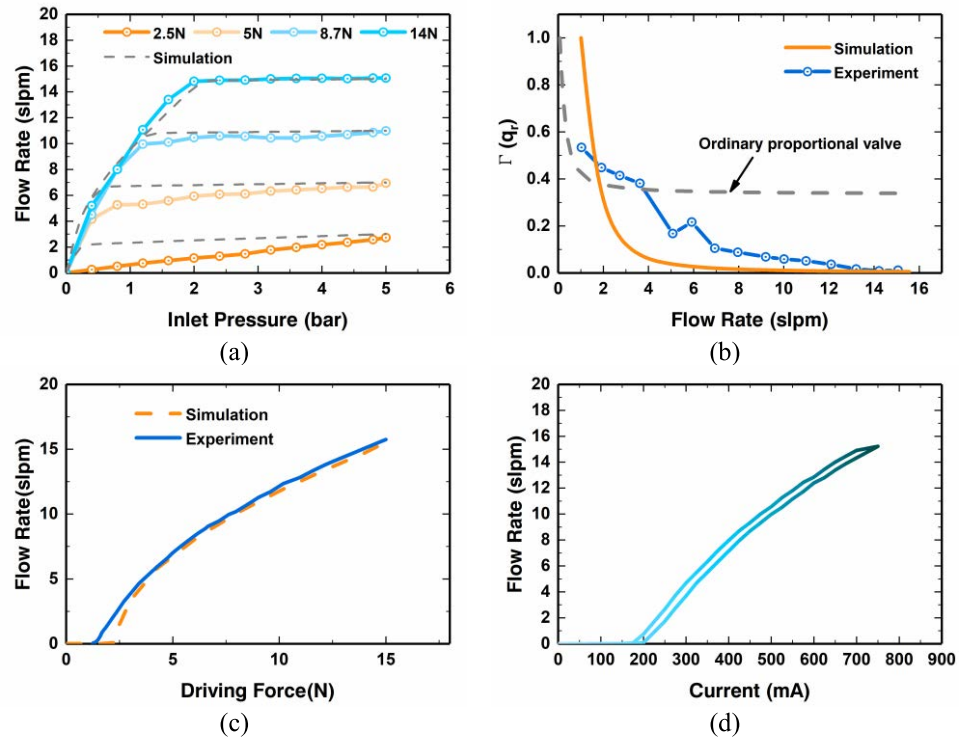

FIGURE 13. (a) Experimentally measured $P_0 - q$ curves for different driving forces. (b) $q_r - \Gamma(q_r)$ curve, comparison between experiment and simulation. (c) $F_I - 1$ curves obtained from experiment and simulation. (d) $I - q$ hysteresis curve of the whole proportional constant flow valve.

the maximum flow change percentage $\Gamma(q_r)$ in the pressure range of 3-5 bar. Because the flow rate increases with inlet pressure, the relationship between $\Gamma(q_r)$ and γ can be expressed by (43). In the formula, γ is written as an expression for the pressure P_0 and the mass flow rate q_r at rated pressure, which can be obtained from (44) and boundary conditions (45). As can be seen from Figure 10(c), the same as the theoretical derivation, the smaller the nozzle diameter, the better the constant flow capability ($\Gamma(q_r)$ for 0.6 mm and 0.7 mm diameters is larger at high flow rates due to the spool displacement beyond the adjustable range). Combining Figures 10(b) and 10(c), we can conclude that the nozzle diameter $d = 0.8$ mm is a more reasonable choice.

$$\Gamma(q_r) = \frac{q_r - q_{low}}{q_r} = \frac{\alpha}{q_r}\int_3^5 \gamma(q_r, P_0)\, dP_0 \tag{43}$$

$$\gamma = \frac{dQ}{dP_{0A}} = \frac{1}{\alpha}\frac{dq_m}{dP_{0A}} = f\left(\frac{q_m}{\alpha}, P_0 - 1.013\right) \tag{44}$$

$$q_m|_{P_0=P_{0r}} = q_r \tag{45}$$

Figure 10(d) shows the spring stiffness versus the feedback hole diameter for a given 15 N driving force, 5 bar inlet pressure and a guaranteed flow rate of 15 slpm. Figure 10(e) shows the variation curves of $\Gamma(q_r)$ with q_r for different feedback hole diameters. Because the nozzle diameter $d = 0.8$ mm is very small, in a larger flow rate range, $\Gamma(q_r)$ increases with the feedback hole diameter. When the nozzle diameter is larger, there is a demarcation point for the effect of feedback hole diameter on $\Gamma(q_r)$, as shown in Figure 10(f). Considering the whole flow rate range, $D = 1.4$ mm and $K \approx 0$ is the most reasonable. The final optimization results are listed in Table 5. The physical object is shown in Figure 11.

TABLE 5. The value of optimization parameters.

Parameter	Valve	Unit
D	1.4	mm
K	Near 0	N/mm
d	0.8	mm

IV. EXPERIMENT

The steady state characteristic test system of the pneumatic proportional constant flow valve with mechanical feedback is shown in Fig. 12. The electromagnet is de-energized, and the driving force is simulated by the gravity of the standard weight. The high-pressure air is filtered by a two-piece, decompressed by a precision pressure regulator, and then enters the valve under test through the inlet. The outlet is connected with a flowmeter to measure the flow rate. By placing different amounts of weight on the armature, the magnitude of the electromagnetic driving force required for different flow rates and the variation of the flow rate with inlet pressure under a given electromagnetic driving force are tested.

Figure 13(a) shows the inlet pressure-flow rate curve for different driving forces measured during the experiment, and figure 13(b) shows the $q_r - \Gamma(q_r)$ curve. We can know that, as the conclusion of theoretical and simulation analysis, the proportional constant flow valve does have a good ability to resist the change of inlet pressure. The constant flow effect of a large flow is better than that of a small flow. Moreover, when the flow rate is high, the experimental results are in good agreement with the simulation results; however, as the flow rate decreases, the gap gradually increases. A possible reason for this is that the feedback membrane has a certain elasticity, and the stiffness of the feedback membrane has a significant influence on the constant flow characteristics at a low flow rate. Manufacturing errors and the deformation of the rubber gasket on the spool are also possible factors. Nevertheless, in half the flow rate range, 7-15 slpm, the flow rate deviation caused by the 40% inlet pressure fluctuation does not exceed 11 %, and the deviation decreases with the increase in flow rate. When the flow rate increases to 15 slpm, the deviation is only about 1.1 %. Compared with an ordinary proportional valve, which has a deviation of approximately 35 % in almost the entire flow range (obtained by simulation), the proportional constant flow valve has obvious advantages. Finally, the driving force-flow rate curve of the proportional constant flow valve and the current-flow rate curve with the electromagnet are shown in Figure 13(c) and Figure 13(d), respectively.

V. CONCLUSION

The structure of a pneumatic proportional constant flow valve with mechanical feedback is introduced. According to theoretical analysis, all forces in the motion equation are related to state variables. The constant flow capability of the valve is analyzed using the steady-state equation of the spool, and the optimal direction is proposed. Through simulation analysis and optimization, the relevant conclusions of the theoretical derivation are verified, and specific values of the optimization parameters are obtained. According to the simulation and relevant experimental tests, the valve has a good proportional constant flow characteristic compared to the ordinary proportional valve, and the constant flow effect at a large flow rate is better than that at a low flow rate. In the flow rate range of 7-15 slpm, the flow rate deviation caused by the 40 % inlet pressure fluctuation is less than 11 %, and the deviation decreases with the increase in flow rate q_r. When the flow rate is increased to 15 slpm, the deviation is only approximately 1.1 %. Finally, the proportional constant current valve is integrated with the electromagnet, and the current-flow rate characteristic curve is tested.

REFERENCES

[1] G. F. Soares, O. M. Almeida, J. W. M. Menezes, S. S. A. Kozlov, and J. J. P. C. Rodrigues, "Air–oxygen blenders for mechanical ventilators: A literature review," *Sensors*, vol. 22, no. 6, p. 2182, Mar. 2022, doi: 10.3390/s22062182.

[2] B. K. Mukkundi, G. Prasad, Y. Gehlot, N. Deval, N. K. Jangir, S. Shetty, G. G. Babu, N. As, V. K. Kakani, and A. Tauheed, "Implementation of conventional air—Oxygen blending in multi-powered continuous positive airway pressure (CPAP) device," in *Proc. 11th Int. Conf. Commun. Syst. Netw. (COMSNETS)*, Jan. 2019, pp. 807–812.

[3] J. Choi, "Flow control system design without flow meter sensor," *Sens. Actuators A, Phys.*, vol. 185, pp. 127–131, Oct. 2012.

[4] H. Wang, X. Wang, J. Huang, and L. Quan, "Flow control for a two-stage proportional valve with hydraulic position feedback," *Chin. J. Mech. Eng.*, vol. 33, no. 1, pp. 1–13, Dec. 2020, doi: 10.1186/s10033-020-00517-4.

[5] E. Chappel, "A review of passive constant flow regulators for microfluidic applications," *Appl. Sci.*, vol. 10, no. 24, p. 8858, Dec. 2020, doi: 10.3390/app10248858.

[6] E. Chappel, "Design and characterization of a passive flow control valve dedicated to the hydrocephalus treatment," *Cogent Eng.*, vol. 3, no. 1, Oct. 2016, Art. no. 1247612, doi: 10.1080/23-311916.2016.1247612.

[7] S. Park, W. H. Ko, and J. M. Prahl, "A constant flow-rate microvalve actuator based on silicon and micromachining technology," in *IEEE Tech. Dig. Solid-State Sensor Actuator Workshop*, Jun. 1988, pp. 136–139.

[8] D. Dumont-Fillon, D. Lamaison, and E. Chappel, "Design and characterization of 3-stack MEMS-based passive flow regulators for implantable and ambulatory infusion pumps," *J. Microelectromech. Syst.*, vol. 29, no. 2, pp. 170–181, Apr. 2020, doi: 10.1109/JMEMS.2019.2962107.

[9] P. Cousseau, R. Hirschi, B. Frehner, S. Gamper, and D. Maillefer, "Improved micro-flow regulator for drug delivery systems," in *Tech. Dig. MEMS 14th IEEE Int. Conf. Micro Electro Mech. Syst.*, Jan. 2001, pp. 527–530.

[10] Q. Zhang, X. Peng, S. Weng, R. Zhang, D. Fang, R. Zhao, and H. J. Qi, "Self-adaptive flexible valve as passive flow regulator," *Extreme Mech. Lett.*, vol. 39, Sep. 2020, Art. no. 100824, doi: 10.1016/j.eml.2020.100824.

[11] S. R. Pawar and V. M. Phalle, "Effect of wear on the performance of hole entry hybrid conical journal bearing employing constant flow valve compensation," *Proc. Inst. Mech. Eng., J, J. Eng. Tribol.*, vol. 233, no. 9, pp. 1277–1292, Sep. 2019, doi: 10.1177/1350650119838078.

[12] Y. Kang, J. Lee, H. Huang, C. Lin, H. Lee, D. Peng, and C. Huang, "Design for static stiffness of hydrostatic plain bearings: Constant compensations," *Ind. Lubrication Tribol.*, vol. 63, no. 3, pp. 178–191, May 2011, doi: 10.1108/00368791111126608.

[13] E. Lisowski and G. Filo, "CFD analysis of the characteristics of a proportional flow control valve with an innovative opening degree shape," *Energy Convers. Manage.*, vol. 123, pp. 15–28, Sep. 2016, doi: 10.1016/j.enconman.2016.06.025.

[14] E. Lisokwi, G. Filo, and J. Rajda, "Pressure compensation using flow forces in a multi-section proportional directional control valve," *Energy Convers. Manage*, vol. 103, pp. 1052–1064, Oct. 2015, doi: 10.1016/j.enconman.2015.07.038.

[15] J. Hu, J. Zhang, L. Suo, and Y. Zheng, "Study on mathematic model of air valve based on real gas characteristics," in *Proc. Design, Anal., Control Diagnosis Fluid Power Syst.*, vol. 4, Jan. 2007, pp. 103–107.

[16] *Pneumatic Fluid Power Components Using Compressible Fluids Determination of Flow Rate Characteristics*, document ISO 6358, 1989.

[17] M. M. Rahman, "Wall-distance-free formulation for SST k-ω model," *Eur. J. Mech. Fluids*, vol. 75, pp. 71–82,May/Jun. 2019, doi: 10.1016/j.euromechflu.2018.11.010.

[18] K. Zhuang, N. Wenchi, and S. Liping, "Application of the improved SST turbulence model for separated flow," *J. Harbin Eng. Univ.*, vol. 38, no. 9, pp. 1359–1364, 2017, doi: 10.11990/jheu.201606063.

SIHAO FU was born in Zhejiang, China, in 1997. He received the bachelor's degree in mechanical design manufacture and automation from Ningbo Tech University, in 2020. He is currently pursuing the master's degree with Zhejiang University. His research interests include pneumatic valve and electromechanical converter for valve.

SHUO LIU received the B.Eng. degree in measurement and control technology from the Huazhong University of Science and Technology, China, in 2009, and the Ph.D. degree in mechatronic control engineering from Zhejiang University, China, in 2014.

From 2015 to 2018, he was a Postdoctoral Researcher at the Ocean Research Center of Zhoushan, Zhoushan, and also at Zhejiang University. Since 2020, he has been an Associate Professor with the Ocean Academy, Zhejiang University. His research interests include high performance hydraulic components and systems, autonomous underwater vehicle, wall-climbing robot, and deep-water hydraulic equipment.

YONG CAI received the M.S. degree in mechanical and electrical engineering from Hangzhou Electronic Science and Technology University, Hangzhou, China, in 2011. He is currently a Senior Engineer with the Zhoushan Ocean Research Center, Zhejiang University, and engaged in the research of marine unmanned equipment and technology, fishery intelligent processing technology and equipment. He has presided one national key special program, two pioneer research and development programs of Zhejiang, and one sub-project of the national key research and development program. He received 12 invention patents by the first right holder and published seven academic papers.

JIAJIE MA received the B.S. and M.S. degrees in mechanical engineering from Northeastern University, Shenyang, China, in 2015 and 2018, respectively. From 2018 to 2020, he was an Engineer at Leadmicro Nano Equipment Technology Company Ltd., Jiangsu, engaged in atomic layer deposition vacuum coating and chemical vapor deposition technology research. Since 2020, he has been working as an Engineer with the Zhoushan Ocean Research Center of Zhejiang University, working in the field related to proportional electromagnet and proportional valve.

ZIJING YU was born in Yunnan, China, in 1998. He received the B.S. degree in electrical engineering and automation from North China Electric Power University, in 2019. He is currently pursuing the master's degree in electronic information with Zhejiang University. His research interests include intelligent control of surface and underwater vehicles.

WENHAN GAO was born in Qingyang, Gansu, in 1997. He received the bachelor's degree in mechanical engineering from the Nanjing University of Aeronautics and Astronautics, in 2019. He is currently pursuing the master's degree in mechanics with Zhejiang University. His research interests include the environmental perception and path planning of AUV.

XIAO ZHANG was born in Shandong, China, in 1996. He received the B.S. degree in biomedical engineering from Northeastern University, in 2018. He is currently pursuing the master's degree in electronic information with Zhejiang University. His research interests include sampling equipment and methods for deep-sea microorganisms.